Applied Surface Science 585 (2022) 152730

Contents lists available at ScienceDirect

Applied Surface Science

journal homepage: www.elsevier.com/locate/apsusc

Full Length Article

A localized study on the influence of surface preparation on the reactivity of cast Al-7Si-1Fe and Al-7Si-2Cu-1Fe alloys and their effect on cerium conversion coating deposition

Salil Sainis [a,*], Caterina Zanella [a,b]

[a] Department of Materials and Manufacturing, School of Engineering, Jönköping University, Gjuterigatan 5, Jönköping 55111, Sweden
[b] Department of Industrial Engineering, University of Trento, via Sommarive 9, Trento 38123, Italy

ARTICLE INFO

Keywords:
Conversion coating
Cerium
Localized deposition
Volta potential
AFM-SKPFM
SEM

ABSTRACT

The spontaneous triggering of cerium-based conversion coating deposition occurs due to active micro-galvanic couple induced local rise in pH at cathodic sites. Since surface preparations prior to conversion coating treatment modify the surface reactivity or the extent of micro-galvanic coupling between the anodic and cathodic phases, they are of crucial importance. While many past works have studied the effect of various preparations including alkaline etching and/or acid pickling and their parameters on the resulting conversion coating, very few studies focus on the local surface reactivity changes from the surface preparation. Moreover, most of the studies use high Cu containing AA2024, and related work on other alloys are scarce. In this study, two model cast alloys Al-7Si-1Fe and Al-7Si-2Cu-1Fe have been created to obtain a relatively homogeneous microstructure containing two different cathodic activity intermetallics Fe-rich IM β-Al_5FeSi and Cu-rich IM θ-Al_2Cu. Changes in the surface state of each alloy are monitored with AFM-SKPFM after subjecting them to four specific surface preparations: (1) Mechanical polishing (2) NaOH etching (3) NaOH etching + HNO_3 Pickling (4) NaOH etching + H_2SO_4 pickling and correlations have been made with localized conversion coating deposit observations.

1. Introduction

The first layer in a multi-layer anticorrosion coating system for aluminium alloys typically is a conversion coating that is in direct contact with the alloy substrate [1]. The surfaces of the 'as-received' aluminium alloys are commonly prepared by different procedures prior to a conversion coating treatment. The as-received surfaces are not very reactive due to the presence of native oxide layer on the aluminium matrix, and it must normally be stripped off for greater reactivity. This is crucial, especially for conversion coatings based on Ce [2], trivalent chromium [3], Ti-Zr [4-7] as their deposition is typically triggered due to active micro-galvanic coupling between the different phases of the microstructure. The deposition mechanism here leverages the localized corrosion phenomenon wherein the micro-galvanic couples between the anodic (typically aluminium matrix) and relatively cathodic sites (typically second phase or intermetallic particles) of the microstructure raises the local pH [8] at cathodic sites to a level sufficient to trigger the precipitation of insoluble conversion compounds.

Among the different local-pH-increase triggered coatings, Cerium-based conversion coatings (CeCC) have been the most widely studied. Furthermore, CeCC offer good corrosion resistance [9,10] and are relatively easy to apply with a dip-immersion method [2]. In this method, the alloy substrate is immersed in an aqueous solution of cerium salts leading to spontaneous deposition of cerium conversion compounds like oxides and hydroxides [11]. Extensive literature exists that describes the mechanism by which the coating is formed, pioneered by Arnott *et al.* [11], Hinton *et al.* [12], and Hughes *et al.* [11,12]. The commonly accepted set of electrochemical reactions involved in the deposition of cerium conversion compounds are the following:

Anodic reaction

Abbreviations: CeCC, Cerium-based conversion coatings; AFM-SKPFM, Atomic force microsopy with scanning Kelvin force microscopy; IM, Intermetallic; OES, Optical emission spectroscopy; SEM, Scanning electron microscopy; SEI, Secondary electron imaging; FIB, Focused ion beam; EDS, Energy dispersive x-ray spectroscopy.

* Corresponding author.at: Department of Materials and Manufacturing, School of Engineering, Jönköping University, Gjuterigatan 5, PO Box 1026, Jönköping SE-551 11, Sweden.
E-mail address: Salil.sanis@ju.se (S. Sainis).

https://doi.org/10.1016/j.apsusc.2022.152730
Received 13 October 2021; Received in revised form 1 February 2022; Accepted 2 February 2022
Available online 5 February 2022

$$Al \rightarrow Al^{3+} + 3e^{-} \quad (1)$$

Cathodic reactions and source of local alkalinity

$$O_2(aq) + 2H_2O + 4e^{-} \rightarrow 4OH^{-}(aq) \quad (2)$$

$$O_2(aq) + 2H_2O + 2e^{-} \rightarrow H_2O_2 + 2OH^{-}(aq) \quad (3)$$

Intermediate complex formation

$$2Ce^{3+} + 2OH^{-} + H_2O_2 \rightarrow 2Ce(OH)_2{}^{2+} \quad (4)$$

$$4Ce^{3+} + O_2 + 4OH^{-} + H_2O \rightarrow 4Ce(OH)_2{}^{2+} \quad (5)$$

Hydroxide precipitation

$$Ce^{3+} + 3OH^{-} \rightarrow Ce(OH)_3 \downarrow \quad (6)$$

Oxide precipitation

$$Ce(OH)_2{}^{2+} + 2OH^{-} \rightarrow CeO_2\downarrow + 2H_2O \quad (7)$$

Due to cathodic nature of intermetallics with respect to the aluminium matrix, several micro-galvanic couples are created across the surface [11] wherein aluminium anode undergoes an oxidation reaction (equation (1)) and the cathodic intermetallic sites support oxygen reduction reaction (equation (2) or (3)) that lead to localized increase in pH. Cerium ions in solution may either exist as standalone Ce^{3+} or form a complex $Ce(OH)_2{}^{2+}$ through reactions (4) and (5). When a sufficiently high pH at cathodic sites is reached, a chemical precipitation reaction of cerium hydroxide and/or cerium oxides occurs through reactions (6) and (7), respectively. The deposition has been shown to initiate locally at strong cathodic sites of the microstructure of aluminium alloys like Cu-rich intermetallic (IM) [12–15] like θ-Al_2Cu and ω-Al_7Fe_2Cu and S-phase IM Al_2CuMg [16,17] and Fe-rich IM like Al_6-(Mn, Fe-Cr) [18] and β-Al5FeSi [19,20].

The activation of micro-galvanic couples is crucial as it creates the necessary condition (local pH increase at cathodic sites) for the triggering of cerium conversion compounds. The amount of local deposition critically depends on the extent of micro-galvanic coupling between the IM and Al matrix, and surface preparation procedures applied prior to the conversion coating treatment influences it. In a study by Campestrini *et al.* [21] on AA2024., it was shown that CeCC deposition did not occur spontaneously even on very active Cu-rich cathodic sites when an as-received surface (prepared with only mechanical polishing) was subjected to conversion coating treatment, due to the anodic aluminium component of the micro-galvanic couple being passive from the native oxide layer over it. The deposition on such a surface did not immediately start but only after initial corrosion reaction occurred wherein Cu dissolved and redeposited uniformly on the surface that provided active sites for the deposition reaction to occur. Studies on another alloy AA6061 [22,23], with non-Cu containing IM, have also reported very slow cerium deposition upon conversion coating treatment of an as-received surface. The surface is typically made more reactive before conversion coating treatment by employing alkaline etching and/or acid "pickling" treatment.

The alkaline etch is a concentrated solution of NaOH which dissolves the native oxide layer as well as Al by the formation of $Al(OH)_4{}^{-}$ ions [24] that go into solution. The etching step also creates an insoluble Al $(OH)_3$ compound smut that tend to adhere to the alloy surface. Acid pickling is then very often further employed to "desmut" the surface off of hydroxides and oxides with acids like HNO_3, H_2SO_4, HF and H_3PO_4 [2]. The surface preparation procedures commonly used before conversion coating deposition tend to be varied and involve either a standalone NaOH etching or a combination of NaOH etching with HNO_3/H_2SO_4/HF pickling. The selection of either standalone etching or a multi-step etching followed by pickling is dictated by the type of alloy.

Cu-rich alloys like AA2024 need surface preparation involving the multi-step process. Rangel *et al.* [23] also showed that the kinetics of CeCC deposition on AA2024 were faster when surface was prepared with alkaline etching in 0.3 wt% NaOH solution and acidic pickling in 25 wt% HNO_3 solution steps as compared to deposition on an as-received surface. Pinc *et al.* [25] further showed that employing alkaline-acid surface preparation (alkaline etching in a commercial Turco-4215 NC LT solution and acid picking in a 1 wt% H_2SO_4 solution) led to greater CeCC deposition as compared to that on a surface prepared with only alkaline etching. Campestrini *et al.* [21] found that the pickling treatment with concentrated H_2SO_4/H_3PO_4 led to attack on Al in the local vicinity of the cathodic IM particles. Cu originating from the selective leaching of Al solid solution and S-phase IM redeposited on the surface creating more active sites that promotes rapid CeCC deposition.

While aerospace alloy AA2024 is the most investigated, there are fewer works studying the effect of surface preparation on conversion coating formation in other non-Cu containing. Study on AA6082 by Decolry *et al.* [26] observed that surface prepared with NaOH etching is the most conducive to CeCC deposition. The microstructure of this alloy is primarily composed of non-Cu containing IM such as $Al_{12}(Fe,Mn)_3Si$, AlMn and AlMnSi [27]. While the conversion coating process was observed to be slow when subjected to only alkaline etching, it was non-existent when the conversion coating treatment was performed after only acidic surface treatment (H_2SO_4/HF). Furthermore, their study involving the influence of sequential NaOH-H_2SO_4/HF and H_2SO_4/HF-NaOH showed that the final etching step should always be one with alkaline solution to obtain any CeCC deposition. In a study on AA1050 clad over AA2024 by Andreeva *et al.* [28], higher deposition kinetics were observed on surface prepared with only NaOH etch than over those surfaces treated with sequential NaOH-HNO_3 surface preparation prior to conversion coating treatment. Heterogeneous coating deposition over surface, preferentially thick over Fe-rich IM in Rheo-High Pressure Die-cast Al-Si alloy was observed in a study by Eslami *et al.* [19] when the preparation involved only NaOH etching step, but no comparison with others was done.

From the literature studies reported in the previous two paragraphs, it becomes evident that the surface preparation procedures cause changes in the surface reactivity, which depends both on the type of surface preparation and the type of alloy. The surface reactivity changes happen from activation of the micro-galvanic couples between the anodic Al and cathodic IM to different extents from the surface preparation procedures. These changes in-turn govern the kinetics of initiation and the evolution of conversion coating formation [29], since the deposition relies heavily on the extent of activation of the micro-galvanic couples. Studies investigating the localized changes in surface reactivity after the different surface preparation procedures are few. One such study by Zhou *et al.*, [29] investigating the kinetics of Zr-based conversion coatings on AA6061 as a function of surface preparation by studying the surfaces under atomic force microscopy with scanning Kelvin probe force microscopy (AFM-SKPFM). They have shown that optimal surface reactivity is obtained with intermediate Δz (height difference of the cathodic phase with the matrix) and high ΔV of the intermetallic particle. Longer exposure to NaOH alkaline etch while increased the Δz, it reduced the ΔV drastically and resulted in slower deposition kinetics. When subjected to HNO_3 preparation step after NaOH, increased simultaneously the Δz and ΔV, but longer exposure increased the Δz too much and resulted in poorer coating deposition than intermediate exposure.

Considering that changes in Δz and ΔV from surface preparation influence the reactivity towards subsequent conversion coating deposition, a localized study is warranted. Local AFM-SKPFM characterizations on AA2024 containing S-phase IM particles are abundant in literature [16,17,30], and very few works investigate other Al alloys. There is a vast majority of other alloys that do not contain the S-phase IM, and in such alloys, the weakly cathodic nature of IM makes the conversion coating treatment of such alloy surfaces challenging. This work therefore investigates two model alloys (Al-7Si-1Fe and Al-7Si-2Cu-1Fe), each of whose microstructure contains different cathodic activity IM and characterizes the local surface reactivity changes after different

surface preparation procedures. The model alloys chosen closely to resemble commonly used hypoeutectic cast Al-7Si alloys used in the automotive industry.

In this work, four types of surface preparation on the two different model alloys have been applied: mechanical polishing, NaOH etching, NaOH etching followed by HNO_3 pickling and NaOH etching followed by H_2SO_4 pickling To understand the effect of each surface preparation step on the surface reactivity and consequently deposition, this research maps the topographical and volta potential on microstructural regions containing specifically the two types of intermetallics: one which contains Cu and is very cathodically active and the other which contains Fe and is relatively less cathodically active. Thus, this study aims at creating new knowledge to the field by investigating intermetallics that have not been studied before using the AFM-SKPFM approach. Furthermore, correlations between surface reactivity changes resulting from four types of preparations and localized conversion coating deposited surface observations have been made.

2. Materials and methods

2.1. Materials

Two model cast Al-Si alloys with additional Fe and/or Cu alloying elements were synthesized for the study. The alloys were created by melting pure aluminium (99.9 wt% Al with 0.1 wt% Fe) with Si, Fe and Cu at 800 ° C in a Nabtherm Tilting Furnace and then ultimately cast into samples by poruing into cylindrical graphite moulds. Before casting the samples of the two models, representative specimens from each melt were first cast as "coins" and three different regions from each coin were characterized with optical emission spectroscopy (OES). Their chemical compositions, as characterized with OES, are respectively listed in Table 1. The values shown in the table are averages ± standard deviation at 95% confidence interval. After casting the samples of the two model alloys, the cylindrical specimens were subjected to remelting (at 780 ° C) and directional solidification in a Bridgeman furnace at a pulling rate of 0.03 mm/s to obtain a relatively controlled microstructure with the desired coarse intermetallic sizes.

2.2. Methods

2.2.1. Sample preparation

Cross sectional discs (ϕ10 mm × 10 mm) were cut from the directionally solidified specimens and cold mounted in a non-conductive epoxy resin of size ϕ30 mm × 20 mm. The samples were first ground with SiC papers up to P4000, followed by polishing with diamond suspension solution in steps of different colloidal particle sizes up to 0.1 μm. They were then rinsed in an acetone bath for 10 min to degrease the surface and remove fine residues from polishing.

2.2.2. Surface preparation before coating treatment

Four different surface preparation procedures were implemented, namely:

(1) Mechanical polishing (as benchmark and referred hereon as "polished")
(2) Mechanical polishing followed by alkaline etching in 0.5 M NaOH solution for 2 min at room temperature (Referred hereon as "NaOH")
(3) Mechanical polishing followed by alkaline etching in 0.5 M NaOH solution for 2 min and then acid pickling in 50 vol% HNO_3 for 30 s (Referred hereon as "NaOH-HNO_3")
(4) Mechanical polishing followed by alkaline etching in 0.5 M NaOH solution for 2 min and then acid pickling in 40 vol% H_2SO_4 for 30 s (Referred hereon as "NaOH-H_2SO_4")

Table 1
Composition of the two model alloys characterized with OES.

Serial number	Designated name	Wt.% Si	Wt.% Cu	Wt.% Fe	Wt.% Al
Model alloy 1	Al-7Si-1Fe	6.79 ± 0.03	–	1.09 ± 0.01	Balance
Model alloy 2	Al-7Si-2Cu-1Fe	6.67 ± 0.11	2.10 ± 0.07	1.05 ± 0.06	Balance

2.2.3. Coating deposition

The conversion coating solution containing 0.1 M $Ce(NO_3)_3$ + 0.1 M NaCl was freshly prepared (pH = 2.8). The different surface prepared samples were immersed in them in separate beakers (ϕ90 mm × 50 mm), each filled with 200 mL of the conversion coating solution at room temperature. The alloy surfaces were immersed in the conversion coating solution at room temperature (25 °C) for up to 18 h. After the given exposure time, the samples were rinsed with distilled water to remove any loosely bound precipitates and placed in a desiccator to dry before being characterized.

2.3. Microstructure and surface characterization

JOEL JSM-7001F scanning electron microscope (SEM) in secondary electron imaging (SEI) mode at 5 kV accelerating voltage was used for characterizing the morphology of different alloy surfaces. Furthermore, TESCAN LYRA3 SEM with Focused Ion Beam (FIB) milling was used to obtain and characterize the cross section of localized deposit regions. The characterization of the cross-section was performed at 15 kV accelerating voltage in SEI mode. To qualitatively characterize the elemental distribution, the microstructure was also mapped with energy dispersive x-ray spectroscopy (EDS) at 20 kV accelerating voltage. The elemental distribution maps show in this study include Al, Si, Cu, Fe and O wherein EDS signal was taken from respective K-shells and Ce wherein EDS signal was taken from L-shell.

Surface topography of the different prepared surfaces and of those with localized deposits was performed using a Park Systems NX10 Atomic Force Microscope (AFM) in non-contact mode. The tip used was PPP-NCSTAu, which is a conductive cantilever coated with Au. Scanning Kelvin Probe Force Microscopy (SKPFM) using the same system was utilized to characterize the local electrochemical properties of the intermetallics.

3. Results and discussion

Cast Al-Si alloys directionally solidify in a dendritic microstructure with primary α-Al dendrites and Al/Si eutectic inter-dendritic region. Intermetallic particles form in the Al/Si eutectic region and with the selected composition, it is expected that the microstructure contains plate-like IM are β-Al_5FeSi and eutectic Si particles in the microstructures of both cast Al-7Si-1Fe and Al-7Si-2Cu-1Fe alloy (Fig. 1). The cast Al-7Si-2Cu-1Fe alloy also contains and additional eutectic phase θ-Al_2Cu IM. The detailed characterization and phase identification using X-ray diffraction is reported in our previous work [31-33].

3.1. Volta potential after different surface preparation procedures

Four surface preparations that are enlisted in Section 2.2, involving alkaline etching and/or acid pickling, were applied prior to CeCC treatment. It is of interest in this study to analyze the local surface changes occurring on the different phases of the microstructure, and to this aim, AFM-SKPFM characterization technique was applied on the same region of the each of the two cast alloys. Fig. 2 and Fig. 6, which shows the topography and volta potential in the polished surface preparation, is used as a benchmark for the two cast alloys Al-7Si-1Fe and Al-7Si-2Cu-1Fe, respectively. Surface characterization performed on the

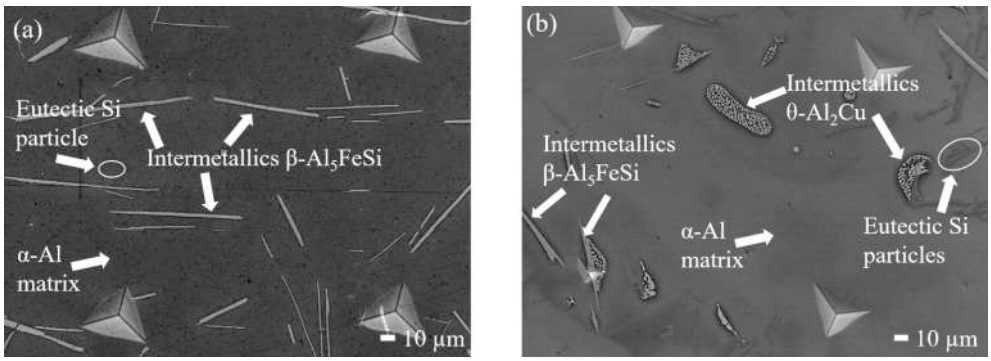

Fig. 1. Microstructure of (a) cast Al-7Si-1Fe alloy and (b) cast Al-7Si-2Cu-1Fe alloy used in the study showing the different phases. Indented grid has a size of 200 μm × 200 μm.

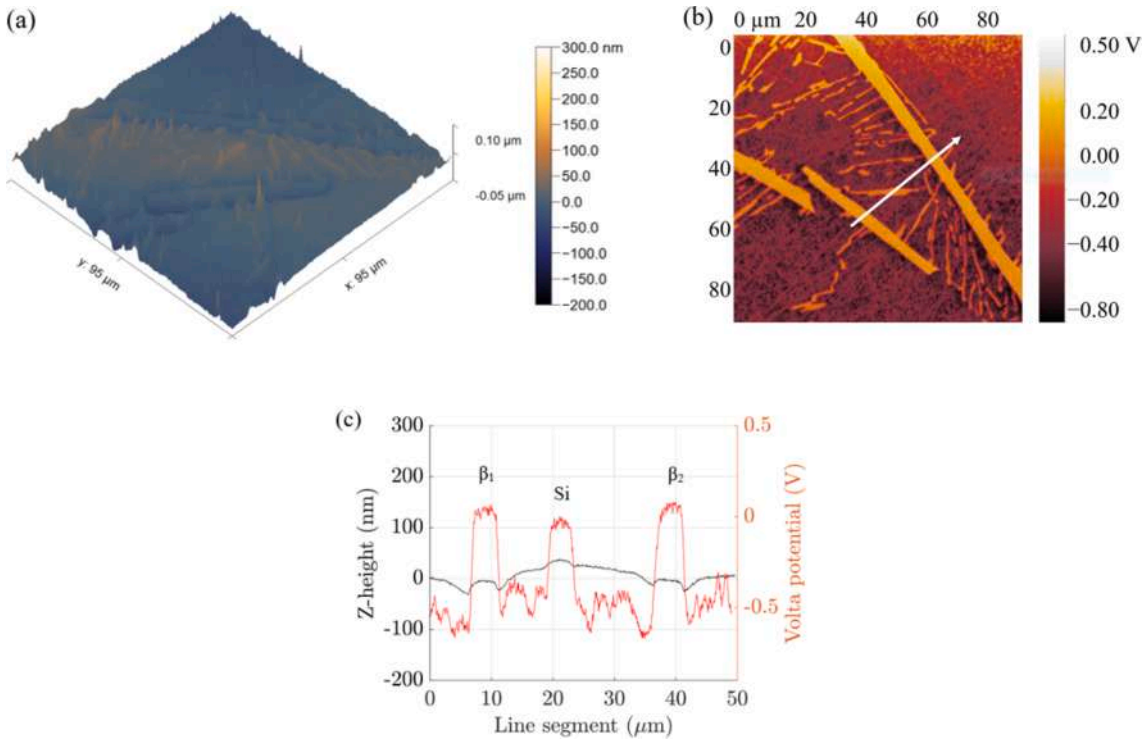

Fig. 2. The mechanically polished surface of cast Al-7Si-1Fe alloy (a) topography with AFM (a) Volta potential map with SKPFM (c) Volta potential (red) and z-height (black) profile along the white line indicated in the volta potential map.

same regions of the two cast alloys after the different surface preparation procedures NaOH, NaOH-HNO_3 and NaOH-H_2SO_4 have been compared with the benchmark to monitor changes in the surface state. The surface states reported subsequently in subsections 3.1.1 and 3.1.2 are further used to explain the surface reactivity after the different surface preparation procedures and compared with the resulting kinetics of deposition reported in section 3.2.

It must be noted that the characterizations reported in Fig. 3, Fig. 4 and Fig. 5 for cast alloy Al-7Si-1Fe and Fig. 7, Fig. 8 and Fig. 9 for cast alloy Al-7Si-2Cu-1Fe were done sequentially on the same region of the microstructure in the respective order. Furthermore, after characterization of the surface after each surface preparation, the samples were mechanically polished very carefully to bring the surface back as close as possible to the "as-received" condition maintaining the same microstructure as characterized in the previous step.

3.1.1. Model cast Al-7Si-1Fe alloy

From the z-height profile of the polished surface condition along the selected white line in Fig. 2 (b) it is seen that the β-IM and eutectic Si particles were elevated ~ 25–30 nm and 20 nm above the aluminium matrix, respectively. This is due to the difference in hardness which makes the different phases abrade to different extents after mechanical polishing. The z-height of β-IM and eutectic Si particles are hereby referred to as Δz_{Fe} and Δz_{Si}, respectively. The volta potential difference reported in this study is calculated from the difference between the volta potential of Al-matrix and each of the different phases (β-IM or eutectic Si particle), and are hereon referred to as ΔV_{Fe} and ΔV_{Si}, respectively. The measurements reported in Table 2 show that the β-IM and eutectic Si particle have a positive volta potential difference indicating that they are both relatively cathodic to the Al-matrix. The values in the table are reported as average ± standard deviation at 95% confidence interval, obtained from three measurements done on the same map.

Upon subjecting the surface to alkaline etching with NaOH solution for two minutes, a greater height difference Δz_{Fe} and Δz_{Si} of 305.90 ± 5.68 nm and 287.4 ± 20.95 nm respectively are observed compared to 22.7 ± 2.67 nm and 14.49 ± 1.92 nm in the mechanically polished

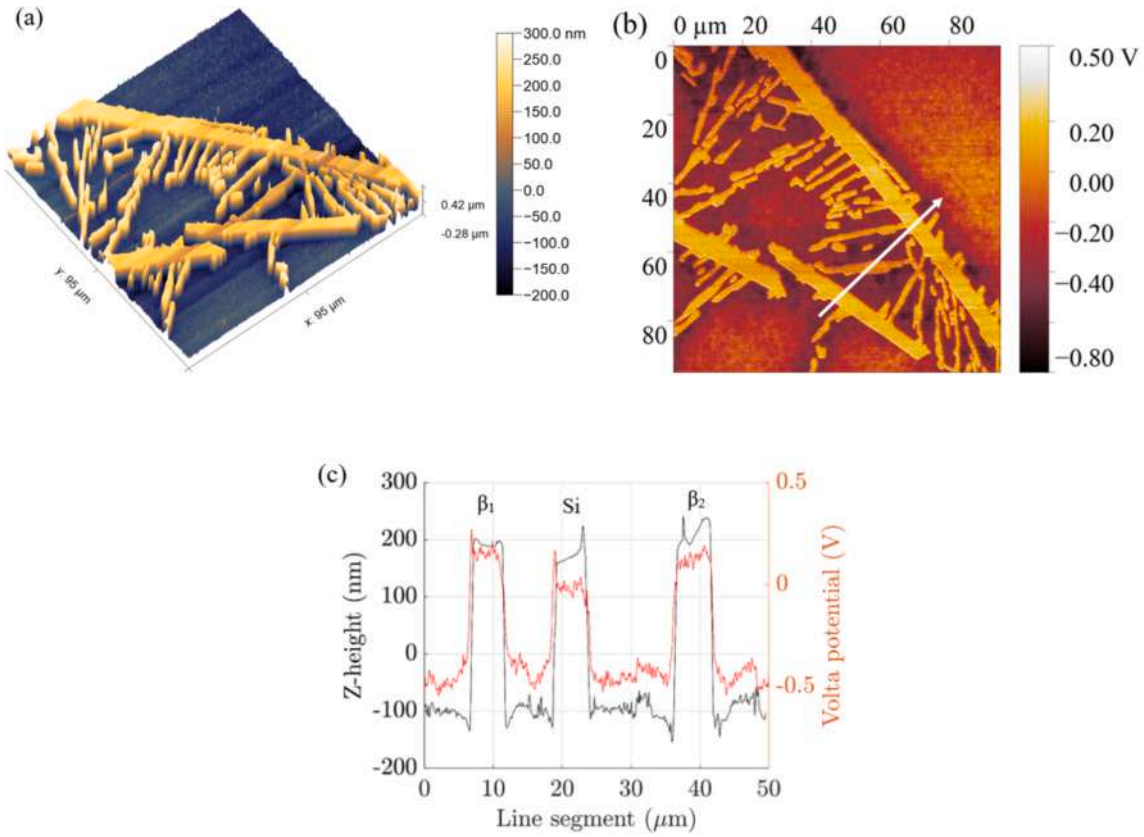

Fig. 3. NaOH etched surface of cast Al-7Si-1Fe alloy (a) topography with AFM (a) Volta potential map with SKPFM (c) Volta potential (red) and z-height (black) profile along the white line indicated in the map.

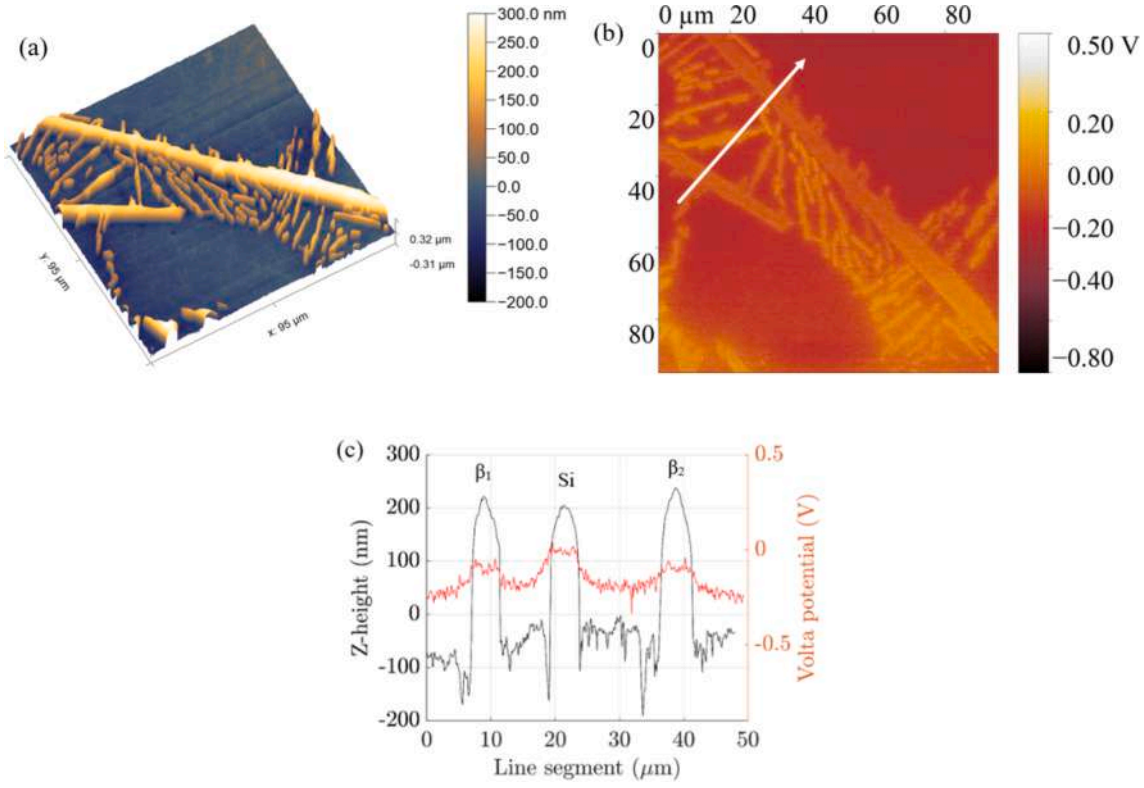

Fig. 4. NaOH-HNO_3 prepared surface of cast Al-7Si-1Fe alloy (a) topography with AFM (a) Volta potential map with SKPFM (c) Volta potential (red) and z-height (black) profile along the white line indicated in the map.

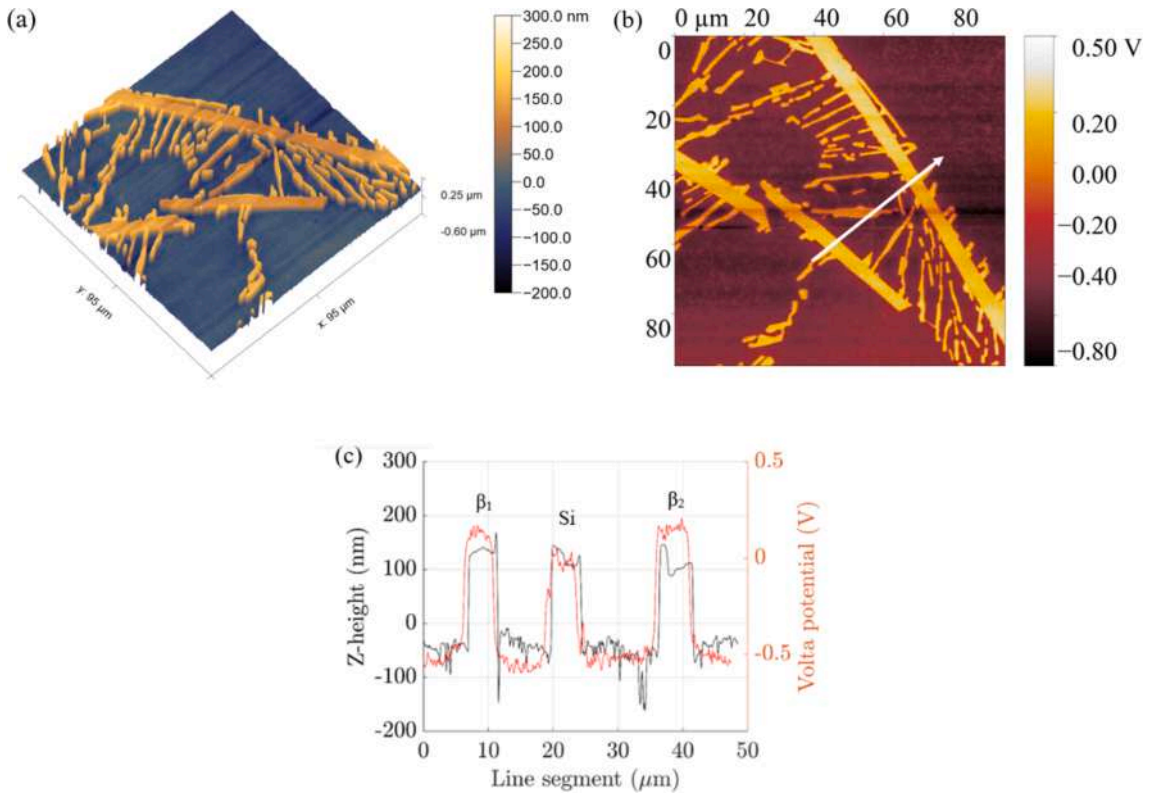

Fig. 5. NaOH-H_2SO_4 prepared surface of cast Al-7Si-1Fe alloy (a) topography with AFM (a) Volta potential map with SKPFM (c) Volta potential (red) and z-height (black) profile along the white line indicated in the map.

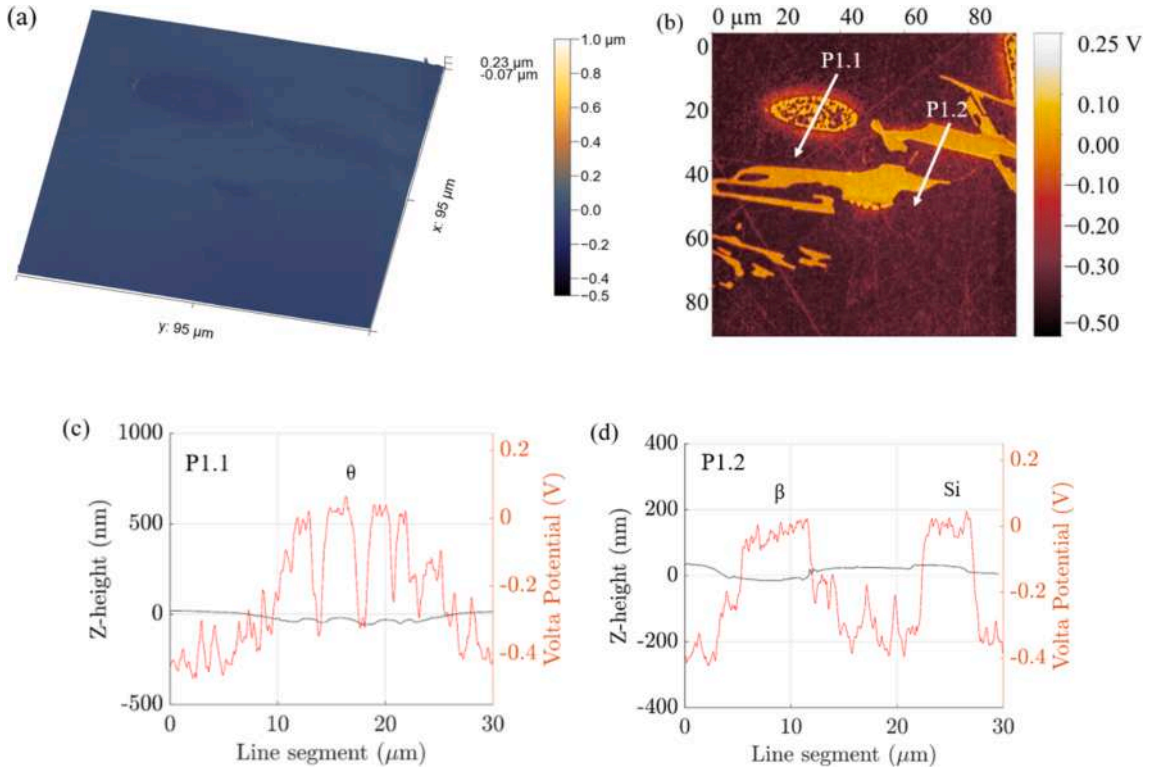

Fig. 6. The mechanically polished surface of cast Al-7Si-2Cu-1Fe alloy (a) topography with AFM (a) Volta potential map with SKPFM (c and d) Volta potential (red) and z-height (black) profile along the white lines P1.1 and P1.2, respectively.

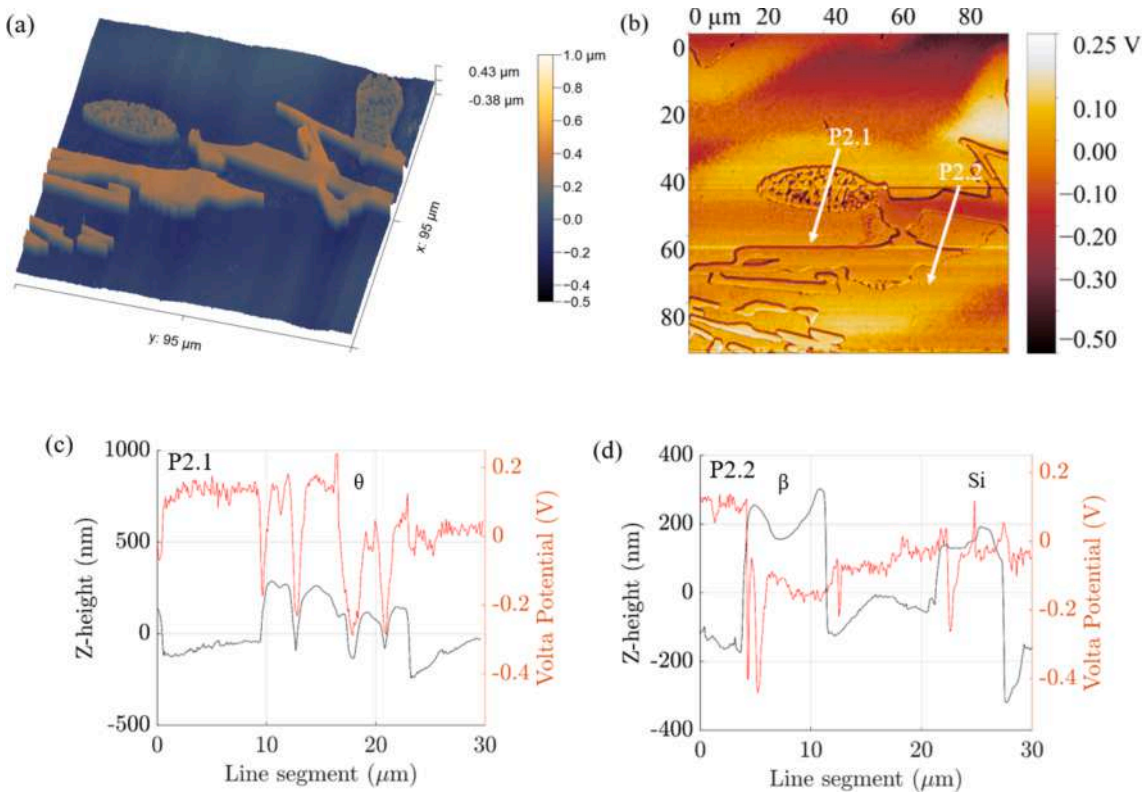

Fig. 7. The NaOH prepared surface of cast Al-7Si-2Cu-1Fe alloy (a) topography with AFM (a) Volta potential map with SKPFM (c and d) Volta potential (red) and z-height (black) profile along the white lines P2.1 and P2.2, respectively.

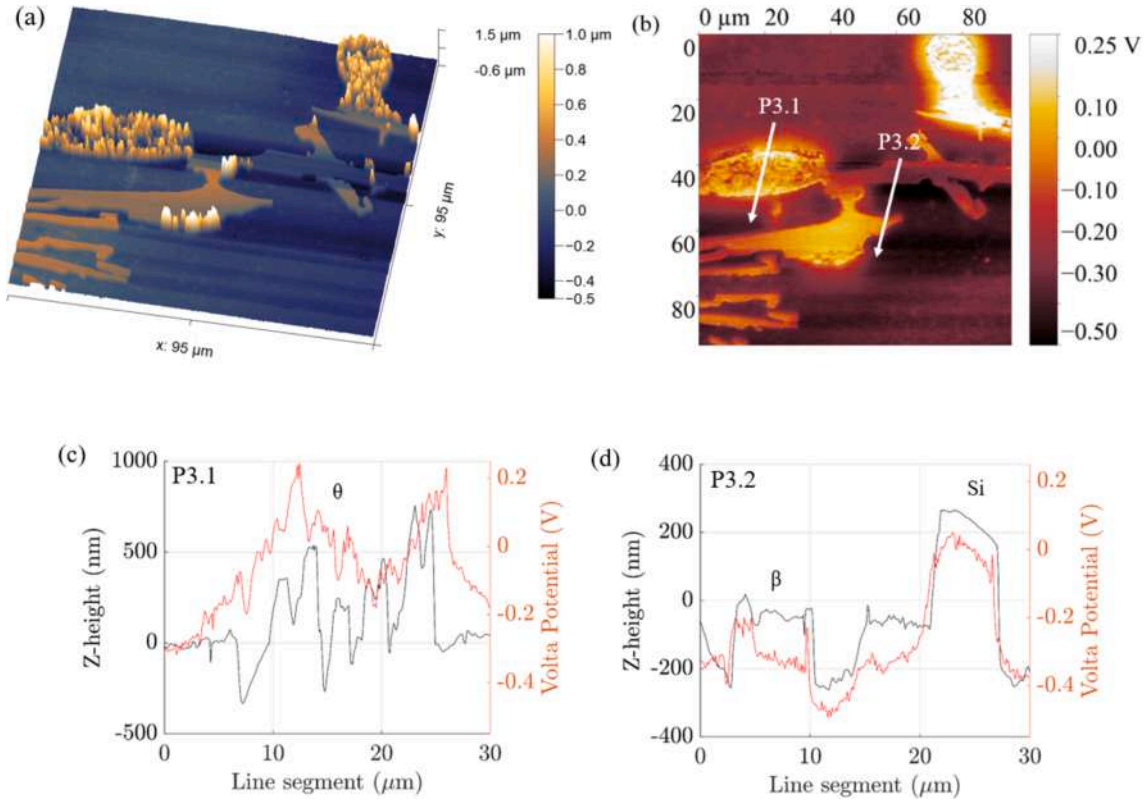

Fig. 8. The NaOH-HNO_3 prepared surface of cast Al-7Si-2Cu-1Fe alloy (a) topography with AFM (a) Volta potential map with SKPFM (c and d) Volta potential (red) and z-height (black) profile along the white lines P3.1 and P3.2, respectively.

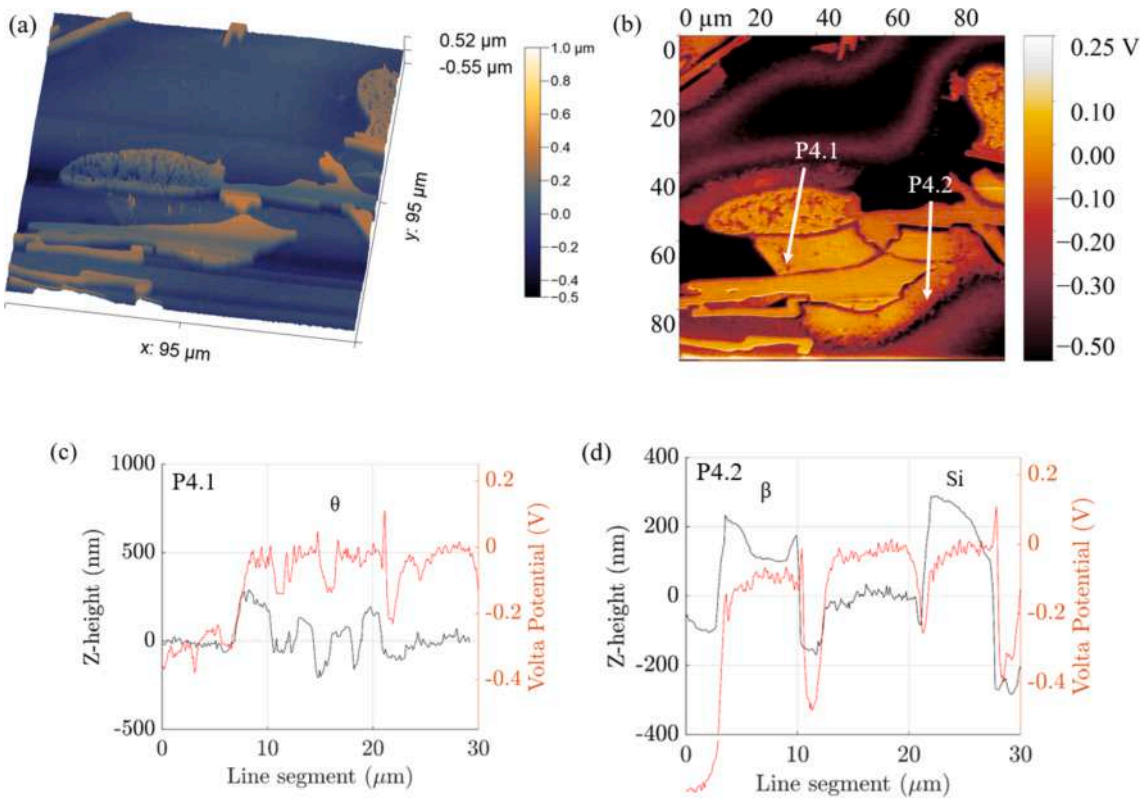

Fig. 9. The NaOH-H_2SO_4 surface of cast Al-7Si-2Cu-1Fe alloy (a) topography with AFM (a) Volta potential map with SKPFM (c and d) Volta potential (red) and z-height (black) profile along the white lines P4.1 and P4.2, respectively.

Table 2
Phase z-height (Δz) and volta potential difference (ΔV) relative to the aluminium matrix of different phases of the Al-7Si-1Fe microstructure after difference.

Physical property	Surface preparation	Phase		
		β_1	Eutectic Si	β_2
Δz	Polished	22.7 ± 2.67	14.49 ± 1.92	9.08 ± 2.57
	NaOH	305.90 ± 5.68	287.4 ± 20.95	333.83 ± 20.59
	NaOH-HNO_3	322.43 ± 20.58	284.90 ± 21.91	289.95 ± 15.95
	NaOH-H_2SO_4	193.15 ± 12.39	172.89 ± 14.08	181.79 ± 22.23
ΔV	Polished	0.66 ± 0.01	0.51 ± 0.01	0.67 ± 0.01
	NaOH	0.70 ± 0.05	0.51 ± 0.05	0.58 ± 0.02
	NaOH-HNO_3	0.14 ± 0.02	0.19 ± 0.02	0.10 ± 0.02
	NaOH-H_2SO_4	0.64 ± 0.04	0.56 ± 0.04	0.64 ± 0.02

condition. NaOH etching removes the native layer of aluminium oxide and dissolves the Al matrix, leaving the β-IM and eutectic Si particles to protrude normal to the surface exhibiting a significant height difference. In this case, the NaOH etching step appears to have removed ~ 250 nm to 270 nm of the material from the matrix and native oxide from the vicinity of the IM. The β-IM and eutectic Si particle were observed to remain cathodically active after NaOH etching with ΔV_{Fe}=+0.70 ± 0.05 V and ΔV_{Si}=+0.51 ± 0.05 V.

When a mechanically polished surface was subjected to NaOH-HNO_3 surface preparation, the β-IM were observed to protrude outward at similar z-heights as seen in the NaOH surface preparation procedure. However, the value of ΔV_{Fe} dropped to + 0.14 ± 0.02 V, and that of ΔV_{Si} also dropped to + 0.19 ± 0.02 V as compared to the much higher ΔV_{Fe} in the previous two surface preparation procedures. A decreased ΔV_{Fe} indicates that the extent of galvanic coupling between the β-IM and Al matrix as well as that of eutectic Si particle and Al matrix was significantly reduced in this surface preparation procedure. HNO_3 is a strong oxidizer and has been shown to passivate iron [34]. Because the β-IM are rich in Fe, the nitric acid pickling step passivated it, leading to the diminishment of ΔV_{Fe}. Such low ΔV_{Fe} compared to that in either mechanical polishing or NaOH surface preparation procedures reduces the extent of mico-galvanic coupling between the phase and the Al-matrix.

In contrast, a mechanically polished surface subjected to acid pickling with another acid, H_2SO_4, after NaOH etching did not appear to reduce the volta potential difference of either of the phases β-IM and eutectic Si particle. A clear difference in the surface state is observed when the cast alloy Al-7Si-1Fe microstructure is subjected to pickling with H_2SO_4 as compared to HNO_3 pickling, both performed after NaOH etching step.

3.1.2. *Model cast Al-7Si-2Cu-1Fe alloy*

The z-height and volta potential map of a microstructural region of the cast alloy is shown in Fig. 6 (a) and Fig. 6 (b), respectively. The Cu-rich θ-IM in the cast Al-7Si-2Cu-1Fe alloy microstructure has a eutectic structure consisting of Al_2Cu and Al. This brings out the non-uniform profile of the volta potential along the line P1.1 in Fig. 6 (b) shown in Fig. 6 (c) as compared to the relatively flat profile along line P1.2 over a β-IM shown in Fig. 6 (d). The regions within the eutectic θ-IM that are Al_2Cu show a greater volta potential as compared to Al in the eutectic. Furthermore, the ΔV of Al in the eutectic θ-IM is observed to be more positive than Al from the bulk matrix. A possible explanation of this lies in the argument that during IM formation, there exists a gradient of alloying elements in the vicinity of the IM due to grain segregation. The Al in the eutectic θ-IM has more Cu in solid solution than bulk Al, causing the eutectic Al to have a more positive ΔV. The volta potential difference of the Al_2Cu in the θ-IM with the Al-matrix will hereon be referred to as ΔV_{Cu}.

Subjecting the sample to alkaline etching in NaOH solution brought

about changes in the topographical z-height and volta potential profile as can be seen from Fig. 7 (a) and Fig. 7 (b), respectively. Localized attack after NaOH etching caused the dissolution of bulk Al matrix as well as the Al in eutectic θ-IM causing the Al_2Cu component to protrude out of the matrix. Different from the observation made in the polished condition, the bulk Al after NaOH etching had similar values of volta potential as that of Al_2Cu in the eutectic θ-IM, but the Al in eutectic had much more negative volta potential values (Fig. 7 (c)). It appears that, because the bulk Al matrix in the vicinity of the IM had similar ΔV values compared to Al_2Cu from the eutectic θ-IM (Fig. 7 (c)), insoluble products of the etching reaction may have settled on the matrix and thus showing such volta potential values. The ΔV of bulk Al far away from the IM were however more negative (Fig. 7 (b)).

Subjecting the polished cast Al-7Si-2Cu-1Fe microstructure to NaOH-HNO_3 surface preparation led to profound changes in the topography (Fig. 8 (a)) and volta potential (Fig. 8 (b)). As can be seen from the Fig. 8 (c), the Al_2Cu from the eutectic θ-IM appeared to protrude out much more than that after just NaOH surface preparation. Moreover, the profile of z-height along line P3.1 on the eutectic θ-IM had more sharp peaks in comparison to the profile (Fig. 7 (c)) on the same IM after NaOH surface preparation. Furthermore, the volta potential profile along the IM in NaOH-HNO_3 (Fig. 8 (c)) condition was significantly different than that in either polished condition (Fig. 6 (c)) or in NaOH etched condition (Fig. 7 (c)). The volta potential profile here was observed to not follow the "shape" of the z-height and appeared to gradually become more positive towards the centre of the eutectic θ-IM. Pickling with HNO_3 removed the "smut" left behind from the NaOH etching reaction and also aggressively dissolved more Al matrix. This led to a greater Δz than that seen in the case of surfaces subjected to only etching surface preparation. Furthermore, removal of the smut by HNO_3 pickling also activated the micro-galvanic couple between the eutectic θ-IM and the Al matrix as measurements (reported in Table 3) show that the IM region has a much more positive volta potential difference compared to that seen in other surface preparation procedures. Another interesting observation is made upon observing the volta potential profile P3.2 along the β-IM (Fig. 8 (d)). Subjecting this IM to NaOH-HNO_3 appears to have greatly reduced the value of ΔV compared to other all other surface conditions. Such an observation made also in subsection 3.1.1 on the same β-IM in cast Al-7Si-1Fe microstructure, strengthens the argument that strongly oxidizing HNO_3 pickling passivates the β-IM.

The NaOH-H_2SO_4 surface preparation procedure did not bring about as drastic changes in the surface state, both in terms of topographical and volta potential, as compared to changes observed after NaOH-HNO_3 surface preparation procedure. The extent of Al_2Cu protrusion out of the Al from the matrix (Fig. 9 (c)) was observed to be at similar levels as seen in the case of surface preparation with just NaOH etching procedure (Fig. 7 (c)). Furthermore, volta potential profile also was similar to the polished and NaOH etched condition, unlike that seen in the case of NaOH-HNO_3 surface preparation. These observations indicate that the extent of selective Al leaching and Cu redeposition, if any, is much less pronounced than in the NaOH-HNO_3 condition.

Table 3
Phase z-height (Δz) and volta potential difference (ΔV) relative to the aluminium matrix of different phases of the Al-7Si-2Cu-1Fe microstructure after difference.

Physical property	Surface preparation	Phase		
		θ	β	Eutectic Si
Δz	Polished	18.10 ± 2.13	3.81 ± 2.28	8.30 ± 3.18
	NaOH	293.71 ± 79.50	387.27 ± 33.57	212.67 ± 27.98
	NaOH-HNO_3	536.46 ± 193.77	192.68 ± 21.65	298.04 ± 27.02
	NaOH-H_2SO_4	215.47 ± 67.29	278.04 ± 30.02	256.87 ± 33.42
ΔV	Polished	0.46 ± 0.03	0.39 ± 0.05	0.40 ± 0.02
	NaOH	0.02 ± 0.01	−0.21 ± 0.02	0.04 ± 0.03
	NaOH-HNO_3	0.42 ± 0.06	0.03 ± 0.04	0.35 ± 0.02
	NaOH-H_2SO_4	0.25 ± 0.01	0.39 ± 0.03	0.25 ± 0.01

3.2. Cerium conversion coating treatment

The localized deposition of CeCC is triggered by the localized rise in pH at cathodic sites. It was shown in previous section that that different surface preparation procedures bring out different local surface states on the cathodic phases of the microstructure. To further prove the validity of the observations made, conversion coating treatment in a cerium nitrate solution have been performed. The most active micro-galvanic couples would show the quickest deposition and also of a higher quantity compared to micro-galvanic couples that are not as active.

3.2.1. On cast Al-7Si-1Fe alloys

The Al-7Si-1Fe cast alloy, after the four surface preparation procedures, was subjected to conversion coating treatment by immersion in a 0.1 M $Ce(NO_3)_3$ + 0.1 M NaCl solution for 18 h. The resulting microstructures of each of the conversion coated surfaces are shown in Fig. 10. From the volta potential characterized in Section 3.1.1, localized CeCC deposits are expected to form over cathodic phases such as β-IM and eutectic Si when the alloy is subjected to conversion coating treatment after surface preparation – polished, NaOH and NaOH-H_2SO_4 as the ΔV_{Fe} shows values more positive than Al matrix. This is expected as more positive ΔV demonstrates a greater cathodic character and thus may cause a sufficient OH^- gradient over these phases due to their ability to reduce oxygen locally. After prolonged conversion coating time of 18 h, however, localized CeCC deposits were observed to form on β-IM only in the case of NaOH surface preparation. Similar localized depositions in the NaOH surface preparation were also observed on Fe-rich IM in other studies such as Eslami *et al.* [20], Decolry *et al.* [26] and Andreeva *et al.* [28] on cast HDPC Al-Si alloy, AA6082 and AA1050 respectively. CeCC deposition was not observed to form locally on β-IM in other surface conditions like polished or NaOH-H_2SO_4, despite volta potential characterization showing they have a cathodic character. As expected, no CeCC deposition was observed on samples that were prepared with NaOH-HNO_3 due to passivation of β-IM from this procedure. Majority of eutectic Si particles did not show any localized CeCC deposition, after conversion coating treatment on any of the four surface preparations. Some regions within the Si particles did appear to show a localized deposit island (Fig. 10 (b) and (c)), respectively for the surface preparations NaOH and NaOH-HNO_3.

The localized and discrete deposit islands as seen in the case of Fig. 10 (b) are cerium-based oxides and hydroxides. Another microstructural region of the same conversion coated surface is presented in Fig. 11 with and EDS characterized elemental distribution map. Preferential localized deposition was observed on the Fe-rich β-IM phases of the microstructure.

3.2.2. On cast Al-7Si-2Cu-1Fe alloys

The four differently prepared surfaces of cast Al-7Si-2Cu-1Fe alloys were subjected to conversion coating treatment in a 0.1 M $Ce(NO_3)_3$ + 0.1 M NaCl solution for different immersion times (1 h, 2 h and 18 h), and the resulting SEM microstructure is shown in Fig. 12. Localized deposition of conversion coating (indicated by white arrows in Fig. 12 (g)) appeared after just 1 h of coating treatment on surfaces prepared with NaOH-HNO_3 procedure. After 2 h conversion coating treatment, NaOH prepared surfaces also showed some Cu-rich θ-IM were activated for localized deposition (Fig. 12 (e)), but the Cu-rich θ-IM of surfaces prepared with mechanical polishing (Fig. 12 (b)) and NaOH-H_2SO_4 remained uncovered (Fig. 12 (k)). After a very prolonged conversion coating treatment of 18 h, localized deposits were eventually observed to form on all Cu-rich eutectic θ-IM of the surfaces that were prepared with NaOH, NaOH-HNO_3 and NaOH-H_2SO_4 procedures (Fig. 12 (f), (i)

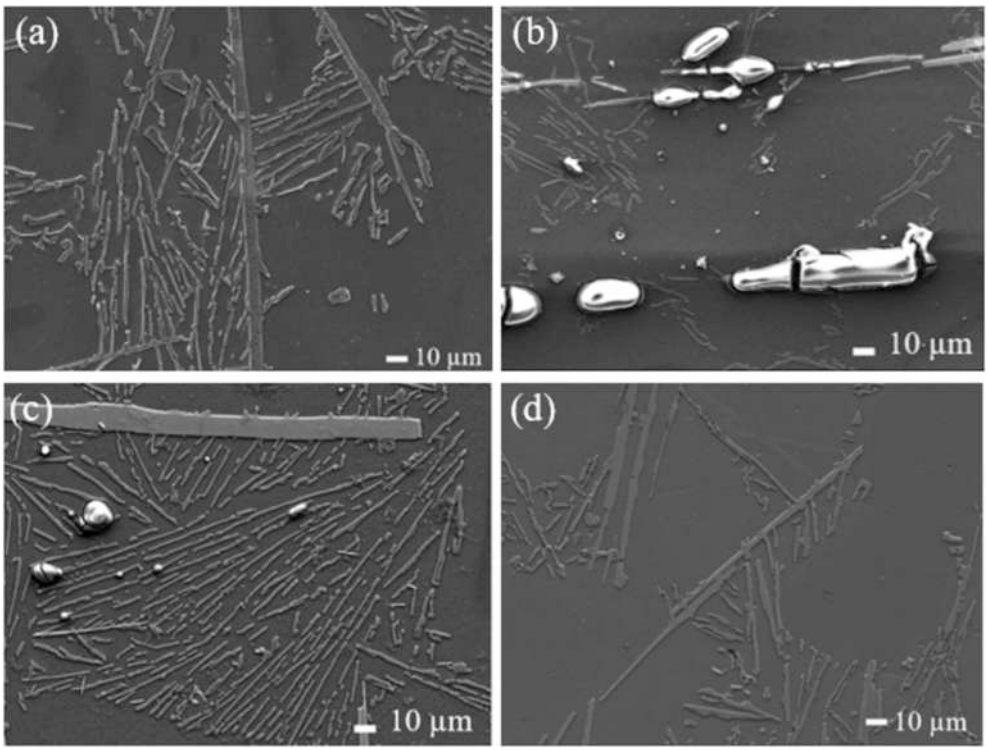

Fig. 10. SEM-SEI micrographs of cast Al-7Si-1Fe alloy surfaces subjected to conversion coating treatment in a 0.1 M $Ce(NO_3)_3$ + 0.1 M NaCl solution for 18 h after the four surface preparations: (a) Polished (b) NaOH (c) NaOH-HNO_3 (d) NaOH-H_2SO_4.

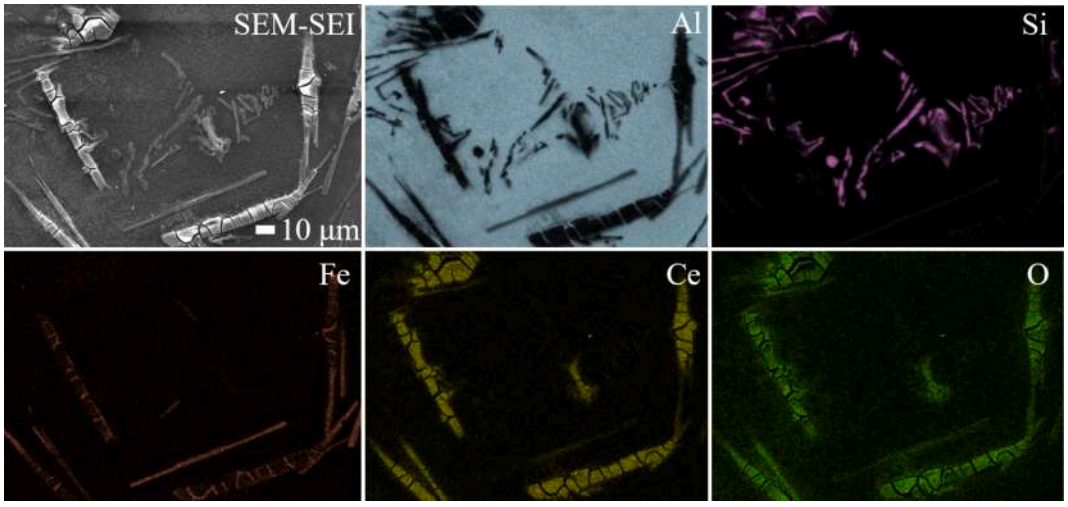

Fig. 11. NaOH prepared cast Al-Si-Fe surface subjected to conversion coating treatment in 0.1 M $Ce(NO_3)_3$ + 0.1 M NaCl solution for 18 h characterized under SEM and showing EDS elemental distribution map.

and (l), respectively). A very small fraction of Cu-rich eutectic θ-IM, however, got covered with a localized CeCC deposit after conversion coating treatment polished surface (Fig. 12 (c)). Sluggish CeCC deposition on as-received (mechanically polished) surfaces has also been reported in studies on high Cu containing AA2024 [21] and low Cu containing AA6061 [22,23].

The conversion coating deposits formed on Cu-rich θ-IM, as shown in Fig. 12 were highly localized on and around the IM. Preferential cerium conversion coating deposition is observed on only the higher cathodic activity Cu-rich θ-IM and not on other phases of the microstructure. FIB milled cross section (Fig. 13) revealed that the deposits were discretely located only on the Cu-rich θ-IM with a thickness of 1.98 µm. In our previous study, we have found that the thickness correlated linearly with the surface area of the underlying IM [31] and thus the thickness of coating observed here is specific to the characterized IM and depends on its size. CeCC have been found in previous studies to be composed of cerium-based oxides and hydroxides [2,11]. Qualitative elemental mapping of the localized deposits using EDS shows that the localized deposit islands are composed of Ce and O based compounds as shown in Fig. 14.

In our previous work [31], we have reported the progression of coating formation with time in the same cast Al-7Si-2Cu-1Fe alloy used in this study and conversion coating treatment after NaOH-HNO_3 surface preparation. It was shown that even after a short conversion coating (30 min), 83% of the eutectic θ-IM showed a localized CeCC deposit and the number increased to 100% eutectic θ-IM coverage after just two h of

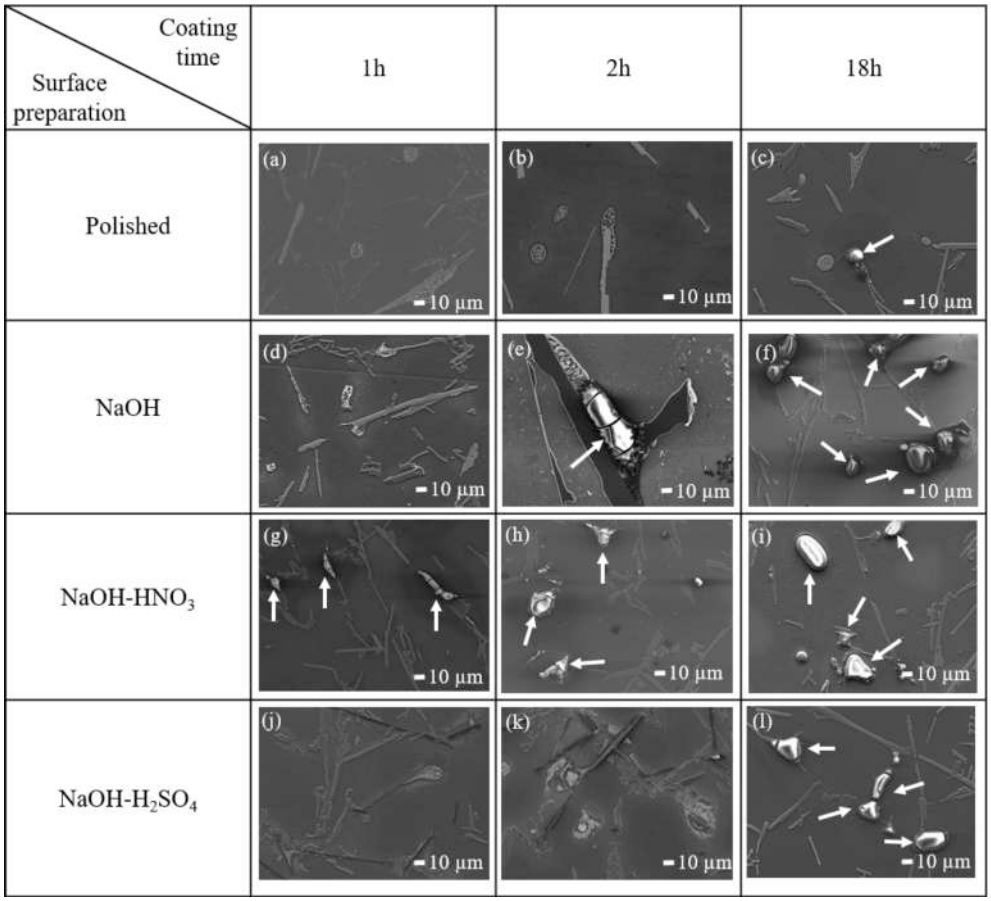

Fig. 12. SEM-SEI characterized microstructure after exposure of cast Al-7Si-2Cu-1Fe alloy to 0.1 M Ce(NO3)3 + 0.1 M NaCl conversion coating solution on different preparation (a,b,c) Polished (d,e,f) NaOH (g,h,i) NaOH-HNO_3 (j,k,l) NaOH-H_2SO_4 for times 1 h, 2 h and 18 h.

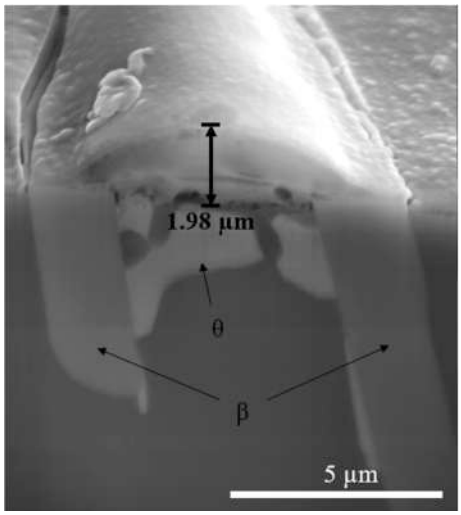

Fig. 13. FIB-SEM cross section of NaOH-HNO_3 prepared Al-7Si-2Cu-1Fe surface subjected to conversion coating treatment for 2 h showing the preferential coating deposition on Cu-rich θ-IM in SEI mode.

conversion coating treatment. Micrograph of the alloy surface after 18 h CeCC treatment is shown in Fig. 12 (c). In this study, when the surface was prepared with polishing, no Cu-rich IM showed deposition at short immersion time up to 2 h (Fig. 12 (b)), however, at 18 h conversion coating treatment, a low fraction of Cu-rich IM showed a localized deposit (Fig. 12 (c)). In the case of CeCC deposition after surface preparation NaOH, very few Cu-rich θ-IM showed deposition at short conversion coating time of 1 h, and with increasing times, a greater fraction of these IM showed a localized deposit. At 18 h, 100% of the Cu-rich IM showed localized CeCC deposition (Fig. 12 (b)). CeCC treatment after NaOH-H_2SO_4 surface preparation showed no deposition at short conversion coating time of 1 h (not shown in figures), but after 18 h all the Cu-rich IM showed localized deposition.

Because a greater fraction of Cu-rich IM was covered with CeCC deposits after the surface preparation NaOH, NaOH-HNO_3 and NaOH-H_2SO_4 compared to the polished surface, it is evident that mechanically polished surface is not very active, likely due to presence of aluminium oxide layer over the matrix which makes the Al-Cu micro-galvanic couple much less active. A few mechanically polished Cu-rich IM were activated for deposition only after 18 h exposure, likely due to a prolonged attack of Cl- ions and breaking of the passivation layer. All other surface preparations, alkaline etching (NaOH) or a combination of alkaline etching and acidic pickling (NaOH-HNO_3 and NaOH-H_2SO_4), activated the surface to different degrees as is observed from the fraction of deposition occurring at different conversion coating times. Surface preparation NaOH-HNO_3 activated the surface the fastest as the implementation of this surface preparation yielded ~ 83% Cu-rich θ-IM coverage after an even shorter 0.5 h conversion coating treatment reported in our previous study [31]. Neither β-IM nor eutectic Si in the cast Al-7Si-2Cu-1Fe microstructure showed any deposition whatsoever even at prolonged conversion coating times.

Upon comparison of the observation made from the AFM-SKPFM analyses in Section 3.1.2 with deposited surfaces, it is evident that the faster deposition kinetics observed on NaOH-HNO_3 prepared surface because such a preparation procedure makes the Cu-rich θ-IM most reactive. In the case of NaOH preparation, however, the micro-galvanic

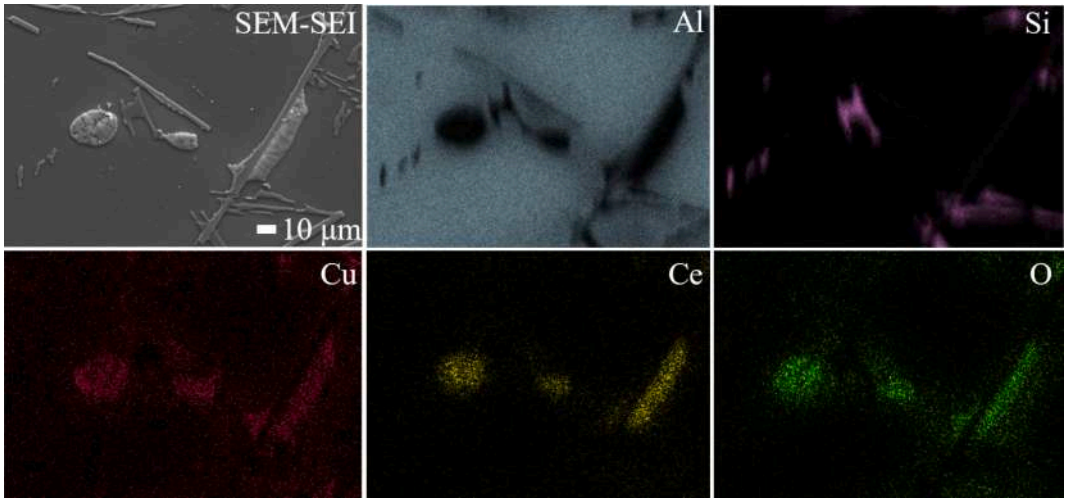

Fig. 14. NaOH-HNO_3 prepared cast Al-Si-Cu-Fe surface subjected to conversion coating treatment in 0.1 M $Ce(NO_3)_3$ + 0.1 M NaCl solution for 2 h characterized under SEM and showing EDS elemental distribution map.

couple between Cu-rich θ-IM and Al matrix is not active. Al may however selectively dissolve during the conversion coating treatment from the attack of Cl^- ions, but this takes time and correlates well with our observation of slower deposition kinetics. Surface preparation NaOH-H_2SO_4, allows redeposition of a smaller fraction of redeposited particles after the pickling step, and this correlates well with the progression of CeCC deposition with time. At shorter conversion coating treatments, no deposition is seen but the surface proceeds to get covered after 18 h.

4. Conclusions

Changes in surface states (topography and volta potential) after four different surface procedures (mechanical polishing, NaOH, NaOH-HNO_3 and NaOH-H_2SO_4) on the same region of two different model alloys Al-7Si-1Fe and Al-7Si-2Cu-1Fe have been reported in this study. Furthermore, conversion coating treatment performed on the different surfaces have been performed and observed to validate the surface reactivity as observed from the AFM-SKPFM measurements. From the study, the following conclusions can be made:

- For cast Al-7Si-1Fe alloys, NaOH preparation brought out beneficial changes in the surface reactivity for the subsequent deposition of conversion compounds. After 18 h conversion coating treatment, cathodic β-IM particles showed a localized CeCC deposition, whereas in other surface preparation conditions, no such deposit was observed.
- NaOH-HNO_3 surface preparation proved deleterious for conversion coating deposition in Al-7Si-1Fe alloys as the strong oxidizing nature of the pickling solution passivated the cathodic Fe-rich β-IM particles. The passivation of β-IM particles was also observed in Al-7Si-2Cu-1Fe alloys subjected to the same surface preparation procedure.
- Cast alloys Al-7Si-2Cu-1Fe reacted strongly to the NaOH-HNO_3 surface preparation procedure and brought surface changes that were most conducive to rapid deposition of CeCC.
- NaOH-H_2SO_4 preparation did not yield an as reactive, if not more, surface compared to NaOH-HNO_3.

CRediT authorship contribution statement

Salil Sainis: Conceptualization, Methodology, Software, Validation, Formal analysis, Investigation, Data curation, Writing – original draft, Writing – review & editing, Visualization. **Caterina Zanella:** Conceptualization, Methodology, Validation, Formal analysis, Investigation, Writing – review & editing, Supervision, Project administration, Funding acquisition.

Declaration of Competing Interest

The authors declare that they have no known competing financial interests or personal relationships that could have appeared to influence the work reported in this paper.

Acknowledgement

The authors sincerely acknowledge the funding received from the European Union's Horizon 2020 research and innovation programme under the Marie Sklodowska-Curie grant agreement No 764977. Ehsan Ghassemali is acknowledged for his help with alloy development and microstructural analyses. Patrick Conway and Johan Börjesson are acknowledged for their help with FIB-SEM sample preparation and characterization.

References

[1] R.L. Twite, G.P. Bierwagen, Review of alternatives to chromate for corrosion protection of aluminum aerospace alloys, Prog. Org. Coat. 33 (2) (1998) 91–100, https://doi.org/10.1016/S0300-9440(98)00015-0.
[2] T.G. Harvey, Cerium-based conversion coatings on aluminium alloys: a process review, Corros. Eng., Sci. Technol. 48 (4) (2013) 248–269, https://doi.org/10.1179/1743278213Y.0000000089.
[3] D.B. Mitton, A. Carangelo, A. Acquesta, T. Monetta, M. Curioni, F. Bellucci, Selected Cr(VI) replacement options for aluminum alloys: a literature survey, Corros. Rev. 35 (2017) 365–381, https://doi.org/10.1515/corrrev-2016-0059.
[4] J.H. Nordlien, J.C. Walmsley, H. Østerberg, K. Nisancioglu, Formation of a zirconium-titanium based conversion layer on AA 6060 aluminium, Surf. Coat. Technol. 153 (1) (2002) 72–78, https://doi.org/10.1016/S0257-8972(01)01663-2.
[5] O. Lunder, C. Simensen, Y. Yu, K. Nisancioglu, Formation and characterisation of Ti–Zr based conversion layers on AA6060 aluminium, Surf. Coat. Technol. 184 (2-3) (2004) 278–290.
[6] X. Zuo, W. Li, S. Mu, J. Du, Y. Yang, P. Tang, Investigation of composition and structure for a novel Ti–Zr chemical conversion coating on 6063 aluminum alloy, Prog. Org. Coat. 87 (2015) 61–68, https://doi.org/10.1016/J.PORGCOAT.2015.05.008.
[7] L. Li, B.W. Whitman, G.M. Swain, Characterization and performance of a Zr/Ti pretreatment conversion coating on AA2024-T3, J. Electrochem. Soc. 162 (6) (2015) C279–C284, https://doi.org/10.1149/2.0901506jes.
[8] L. Li, A.L. Desouza, G.M. Swain, In situ pH measurement during the formation of conversion coatings on an aluminum alloy (AA2024), Analyst. 138 (2013) 4398–4402, https://doi.org/10.1039/c3an00663h.
[9] D.R. Arnott, B.R.W. Hinton, N.E. Ryan, Cationic-film-forming inhibitors for the protection of the AA 7075 aluminum alloy against corrosion in aqueous chloride solution, Corrosion 45 (1) (1989) 12–18, https://doi.org/10.5006/1.3577880.
[10] H. Shih, F. Mansfeld, in: New Methods for Corrosion Testing of Aluminum Alloys, ASTM International, 100 Barr Harbor Drive, PO Box C700, West Conshohocken, PA 19428-2959, 1992, pp. 180–180-16, https://doi.org/10.1520/STP19589S.

[11] D.R. Arnott, N.E. Ryan, B.R.W. Hinton, B.A. Sexton, A.E. Hughes, Auger and XPS studies of cerium corrosion inhibition on 7075 aluminum alloy, Appl. Surf. Sci. 22–23 (1985) 236–251, https://doi.org/10.1016/0378-5963(85)90056-X.
[12] B.R.W. Hinton, D.R. Arnott, N.E. Ryan, Cerium conversion coatings for the corrosion protection of aluminium, Mater. Forum 9 (1986) 162–173.
[13] A.E. Hughes, R.J. Taylor, B.R.W. Hinton, L. Wilson, XPS and SEM characterization of hydrated cerium oxide conversion coatings, Surf. Interf. Anal. 23 (7-8) (1995) 540–550, https://doi.org/10.1002/sia.740230714.
[14] A.E. Hughes, J.D. Gorman, P.J.K. Paterson, The characterisation of Ce-Mo-based conversion coatings on Al-alloys: part I, Corros. Sci. 38 (11) (1996) 1957–1976, https://doi.org/10.1016/S0010-938X(96)00088-1.
[15] A.J. Aldykiewicz, A.J. Davenport, H.S. Isaacs, Studies of the formation of cerium-rich protective films using X-ray absorption near-edge spectroscopy and rotating disk electrode methods, J. Electrochem. Soc. 143 (1) (1996) 147–154, https://doi.org/10.1149/1.1836400.
[16] A. Kolics, A.S. Besing, P. Baradlai, A. Wieckowski, Cerium deposition on aluminum alloy 2024–T3 in acidic NaCl solutions, J. Electrochem. Soc. 150 (11) (2003) B512, https://doi.org/10.1149/1.1615995.
[17] K.A. Yasakau, M.L. Zheludkevich, S.V. Lamaka, M.G.S. Ferreira, Mechanism of corrosion inhibition of AA2024 by rare-earth compounds, J. Phys. Chem. B 110 (11) (2006) 5515–5528, https://doi.org/10.1021/jp0560664.
[18] M.A. Arenas, M. Bethencourt, F.J. Botana, J. de Damborenea, M. Marcos, Inhibition of 5083 aluminium alloy and galvanised steel by lanthanide salts, Corros. Sci. 43 (1) (2001) 157–170, https://doi.org/10.1016/S0010-938X(00)00051-2.
[19] M. Eslami, M. Fedel, G. Speranza, F. Deflorian, N.-E. Andersson, C. Zanella, Study of selective deposition mechanism of cerium-based conversion coating on Rheo-HPDC aluminium-silicon alloys, Electrochim. Acta 255 (2017) 449–462, https://doi.org/10.1016/J.ELECTACTA.2017.09.182.
[20] M. Eslami, M. Fedel, G. Speranza, F. Deflorian, C. Zanella, Deposition and characterization of cerium-based conversion coating on HPDC low Si content aluminum alloy, J. Electrochem. Soc. 164 (9) (2017) C581–C590, https://doi.org/10.1149/2.1511709jes.
[21] P. Campestrini, H. Terryn, A. Hovestad, J.H.W. de Wit, Formation of a cerium-based conversion coating on AA2024: relationship with the microstructure, Surf. Coat. Technol. 176 (3) (2004) 365–381, https://doi.org/10.1016/S0257-8972(03)00743-6.
[22] A.S. Hamdy, A.M. Beccaria, Effect of surface preparation prior to cerium pre-treatment on the corrosion protection performance of aluminum composites, J. Appl. Electrochem. 35 (5) (2005) 473–478, https://doi.org/10.1007/s10800-004-8330-x.
[23] C.M. Rangel, T.I. Paiva, P.P. da Luz, Conversion coating growth on 2024–T3 Al alloy. the effect of pre-treatments, Surf. Coat. Technol. 202 (14) (2008) 3396–3402.
[24] K.J.H. Nelson, A.E. Hughes, R.J. Taylor, B.R.W. Hinton, L. Wilson, M. Henderson, Characterisation of aluminium alloys after HNO3/HF-NaoH-HNO3/HF pretreatment, Mater. Sci. Technol. 17 (10) (2001) 1211–1221, https://doi.org/10.1179/026708301101509287.
[25] W. Pinc, S. Geng, M. O'Keefe, W. Fahrenholtz, T. O'Keefe, Effects of acid and alkaline based surface preparations on spray deposited cerium based conversion coatings on Al 2024–T3, Appl. Surf. Sci. 255 (7) (2009) 4061–4065.
[26] A. Decroly, J.-P. Petitjean, Study of the deposition of cerium oxide by conversion on to aluminium alloys, Surf. Coat. Technol. 194 (1) (2005) 1–9.
[27] T. Khelfa, J.A. Muñoz-Bolaños, F. Li, J.M. Cabrera-Marrero, M. Khitouni, Microstructure and mechanical properties of AA6082-T6 by ECAP under warm processing, Met. Mater. Int. 26 (8) (2020) 1247–1261, https://doi.org/10.1007/s12540-019-00388-y.
[28] R. Andreeva, E. Stoyanova, A. Tsanev, D. Stoychev, Influence of the surface pre-treatment of aluminum on the processes of formation of cerium oxides protective films, J. Phys. Conf. Ser. 700 (2016) 012049, https://doi.org/10.1088/1742-6596/700/1/012049.
[29] P. Zhou, Y. Liu, L. Liu, B. Yu, T. Zhang, F. Wang, Critical role of pretreatment on the corrosion resistance of Zr conversion coating on 6061 aluminum alloy: the combined effect of surface topography and potential difference between different phases, Surf. Coat. Technol. 377 (2019) 124904, https://doi.org/10.1016/j.surfcoat.2019.124904.
[30] L. Lacroix, L. Ressier, C. Blanc, G. Mankowski, Combination of AFM, SKPFM, and SIMS to study the corrosion behavior of S-phase particles in AA2024-T351, J. Electrochem. Soc. 155 (4) (2008) C131, https://doi.org/10.1149/1.2833315.
[31] S. Sainis, S. Roșoiu, E. Ghassemali, C. Zanella, The role of microstructure and cathodic intermetallics in localised deposition mechanism of conversion compounds on Al (Si, Fe, Cu) alloy, Surf. Coat. Technol. 402 (2020) 126502, https://doi.org/10.1016/j.surfcoat.2020.126502.
[32] S. Sainis, C. Zanella, A study of the localized ceria coating deposition on Fe-rich intermetallics in an AlSiFe cast alloy, Materials 14 (2021) 3058, https://doi.org/10.3390/ma14113058.
[33] S. Sainis, The influence of Al alloy microstructure on conversion coating formation, 978-91-87289-63-7 (print), 2021.
[34] H.H. Uhlig, T.L. O'Connor, Nature of the passive film on iron in concentrated nitric acid, J. Electrochem. Soc. 102 (10) (1955) 562, https://doi.org/10.1149/1.2429913.